Research Article Vol. 57, No. 10 / 1 April 2018 / Applied Optics 2597

applied optics

Optical measurements of dynamic wetting and dynamic contact angle

Liping Hou,[1] Xiaodong Yang,[2] Jianxia Qi,[1,3] and Runcai Miao[1,*]

[1]Institute of Physics and Information Technology, Shaanxi Normal University, Xi'an 710062, China
[2]School of Electronic Engineering, Xi'an Shiyou University, Xi'an 710065, China
[3]Department of Applied Mathematics and Applied Physics, Xi'an Institute of Post and Telecommunication, Xi'an 710061, China
*Corresponding author: rcmiao@snnu.edu.cn

Received 7 December 2017; revised 26 February 2018; accepted 28 February 2018; posted 28 February 2018 (Doc. ID 315172); published 28 March 2018

We present a method of optical measurement of the dynamic wetting, the dynamic contact angles, and the changes of the dynamic curved liquid surface corresponding to dynamic wetting, which uses the critical light reflection from dynamic curved liquid surfaces due to the dynamic wetting. When an expanded and collimated laser beam impinges on the dynamic curved liquid surfaces at glancing incidence, the special reflection patterns, which correspond to the different states of the dynamic wetting, are observed. Based on an analytic relation between the bright/dark region width and the height of down-/up-curved liquid surfaces, we proposed a method of optical measurement. In the experiment, a rod such as iron, copper, or aluminum is immersed at constant speed ($u = 0.2$ mm/s) into a liquid bath and withdrawn out gradually. We measured the changing curve of the dynamic contact angle of the iron rod and the characterization of the dynamic curved liquid surface of the iron rod.

OCIS codes: (000.2170) Equipment and techniques; (120.1680) Collimation; (120.5700) Reflection; (240.6648) Surface dynamics.

https://doi.org/10.1364/AO.57.002597

1. INTRODUCTION

Contact angle measurement is an important tool in many areas of applied science and engineering. It is well known that studies of wettability, adhesion, adsorption, and flotation require parameters of the contact angle [1,2]. It would reflect the wettability at the case of balance because the static contact angle is measured under the equilibrium, but it cannot study the relationship between the surface structure and the wettability of the material, the change information of the surface structure, and the precise regulation of the surface structure. However, the dynamic contact angle can provide information such as the roughness of the surface of the material, the uniformity of the chemical properties, and the reconstruction of the hydrophilic/hydrophobic segments [3–5].

We studied the contact angle of a Wilhelmy plate by using optical reflection [6]. In our previous investigation we did not perform to measure the dynamic contact angle of a Wilhelmy plate/rod. The Wilhelmy rod method is generally accepted as the standard technique for measuring the dynamic contact angles [7–9]. A rod as a test solid is immersed at constant speed into a liquid bath and withdrawn out gradually. Due to the dynamic wetting behavior, the dynamic curved liquid surfaces are formed around the rod [10–14]. Generally speaking, particular reflection patterns are experimentally observed when an expanded and collimated laser beam impinges obliquely on the dynamic curved liquid surfaces at glancing incidence. Once the detected liquid surface shows a certain reflectivity for the incident light, it is possible to measure the surface deformation by determining the change of the reflected light from the surface, no matter if the liquid is colorless or colored. Hence the optical reflection technique is a choice for investigating this surface deformation [6,15–17].

A relatively simple technique for measuring the dynamic contact angle of the Wilhelmy rod based on analyzing the reflective patterns is developed. The relation of the dark region width and the maximal height of the up-curved liquid surface is derived theoretically [6]. And the relation of the bright region width and the maximal depth of the down-curved liquid surface is also derived theoretically. As a result, this technique is particularly suitable for the precise measurement of the dynamic contact angle of the Wilhelmy rod. Then the two-dimensional dynamic curved liquid surface profiles are calculated numerically by MATLAB software [18]. It is believed that the critical reflection field is capable of real-time characterization of the dynamic curved liquid surface.

2. EXPERIMENT AND RESULTS

A schematic diagram of the experiment is shown in Fig. 1. Light from a 20 MW He–Ne laser ($\lambda = 632.8$ nm) is

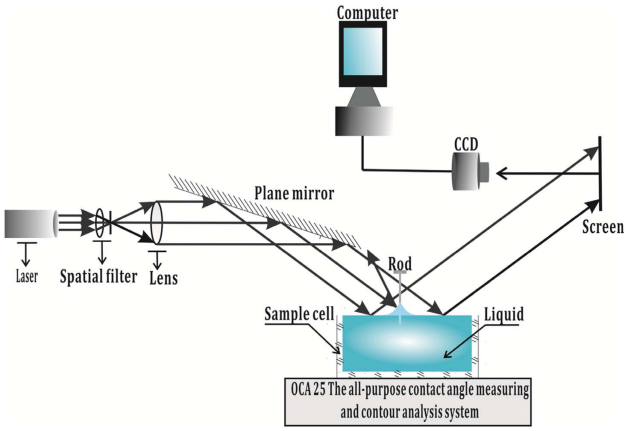

Fig. 1. Schematic diagram of the experimental setup used to study the dynamic curved liquid surface.

expanded and collimated and then used to obliquely illuminate the horizontal free liquid surface at an extremely small glancing angle. Distilled water is first used as the tested liquid. The liquid sample cell is filled by distilled water to a depth of about 3 cm. Several rods of different materials, such as copper, iron, and aluminum, are used in the experiment. The rod, 0.80 mm in diameter, is immersed at constant speed into the liquid and withdrawn out at the center of the illuminated area. The rod is installed on a movable holder of the optical contact angle measuring device (OCA) so that the position of the rod and velocity of rod movement can be adjusted [19]. The liquid sample cell is put on a sample stage of the OCA for capturing the stable and clear reflection patterns. A charge-coupled device (CCD) (MER-132-30UM-L) is used to capture the reflection pattern on a viewing screen. The reflection pattern is from the curved liquid surface around the immersing/withdrawing rod. The distance between the position of the rod and the screen is 1.87 m. The data detected by the CCD are input into a computer. Of course, the reflection pattern can be displayed, stored, and processed by the computer. The room temperature recorded is 20°C. The entire experimental setup including the optical system is set on an optical table equipped with pressurized air supports to minimize the possible effect of ambient vibrations.

The parts of the special patterns reflected from dynamic curved liquid surface around the immersing/withdrawing rod at a small glancing angle on the screen are shown in Figs. 2 and 3.

When a rod such as copper, glass, or aluminum is vertically immersed into liquid water at a constant speed, the liquid climbs up the rod at first, then the liquid surface becomes curved down with the depth of the immersing rod. Figures 2(a)–2(h) show the reflection patterns, respectively, corresponding to the rod immersed into the liquid at different moments. In the experiment, the CCD is used to capture the reflection pattern in succession, then select the reflection pattern at 15 s [see Fig. 2(a)]. The corresponding reflection pattern is selected every 15 s for eight intervals [see Figs. 2(a)–2(h)]. First, Fig. 2(a) shows the reflective light intensity that results from the up-curved surface at 15 s. The pattern contains a dark central region and a bright field outside. The shape of the dark

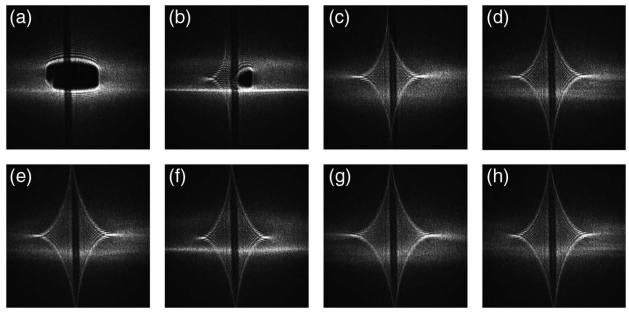

Fig. 2. Part of special patterns reflected from the dynamic curved liquid surface around the immersing rod.

field is close to an ellipse. Clear fringes, like single-edge diffraction, are observed near the boundary between the dark and bright fields. Figure 2(b) shows the reflective light intensity that results from the curved surface at 30 s. One part of the reflection pattern contains a dark central region and a bright field outside. The shape of the dark field is close to an ellipse. Clear fringes, like single-edge diffraction, are observed near the boundary between the dark and bright fields, and the other part contains the bright central region and a weaker field outside. The fringes can be observed in the central range. Finally, Figs. 2(c)–2(h) show the reflective light intensity that results from the down-curved surface between 45 s and 120 s every 15 s for five intervals. The pattern contains the bright central region and a weaker field outside. The fringes can be observed in the central range.

On the contrary, when a rod such as copper, glass, or aluminum is vertically withdrawn out of liquid water at a constant speed, the liquid surface curves down at first, then the liquid surface becomes curved up with the height of the withdrawing rod. Figures 3(a)–3(h) show the reflection patterns, respectively, corresponding to the rod withdrawing out of the liquid at different moments. In the experiment, the CCD is used to capture the reflection pattern in succession. Then we select the reflection pattern at 135 s [see Fig. 3(a)]. The corresponding reflection pattern is selected every 15 s for eight intervals [see Figs. 3(a)–3(h)]. First, Figs. 3(a) and 3(b) show the reflective light intensity that results from down-curved surface between 135 s and 150 s every 15 s for one interval. The pattern contains the bright central region and a weaker field outside.

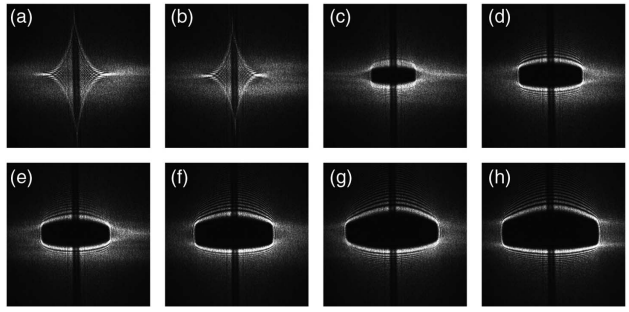

Fig. 3. Part of special patterns reflected from the dynamic curved liquid surface around the withdrawing rod.

The fringes can be observed in the central range. Finally, Figs. 3(c)–3(h) show the reflective light intensity that results from the up-curved surface between 165 s and 240 s every 15 s for five intervals. The pattern contains a dark central region and a bright field outside. The shape of the dark field is close to an ellipse. Clear fringes, like single-edge diffraction, are observed near the boundary between the dark and bright fields.

3. THEORETICAL ANALYSIS

Let us discuss the formation of the special patterns reflected from the dynamic curved liquid surface, respectively, in Fig. 3 using geometric optics. The liquid surface becomes curved down. The profile of the liquid surface at a certain time is formed, as shown in Fig. 4. A parallel laser beam illuminates the down-curved liquid surface at an extremely small glancing angle (less than 5°). The reflected rays 2 and 4 reflect from the down-curved liquid surface. The parallel reflected rays 1 and 5 reflect from the free liquid surface. The rays 1 and 5 reach the down-curved liquid surface at O_1 and O_2, respectively. In particular, the reflected ray 3 reflects from the critical depth of the down-curved liquid surface. The rays 1′ and 5′ are the boundary rays. Rays 3′ and 1′ intersect at the lowest point. There will be reflection in the range between rays 1′ and 5′ and they form a bright region on the observation, which was shown in Figs. 2(a) and 3(c)–3(h). Taking the theoretical analysis above into consideration, the optical measurement can be shown in Fig. 4. From the geometry of Fig. 4 the relation of the critical depth of the down-curved liquid surface, the bright region width on the screen, the angle between the horizontal plane and the tangent at the depth point of the down-curved liquid surface, and the glancing angle are simply derived. Thus, the relationship can be written in the form as follows:

$$h = \frac{l \tan\left(\frac{\varphi}{2}\right)}{\tan(\varphi + 2\theta') - \tan\left(\frac{\varphi}{2}\right)}, \tag{1}$$

where h is the relation of the critical depth of the down-curved liquid surface, l is the bright region width on the screen, θ' is the angle between the water surface normal and the tangent at the depth point of the down-curved liquid surface, and φ is the glancing angle.

Figure 4 indicates the measurement of the critical depth h in a similar manner. When the liquid surface becomes curved up, the profile of the liquid surface at a certain time is formed, as shown in Fig. 5. A parallel laser beam illuminates the up-curved liquid surface at an extremely small glancing angle (less than 5°). The reflected ray 3 reflects from the up-curved liquid surface. The parallel incident rays 1, 2, 4, and 5 reflect from the free liquid surface. The rays 2 and 4 reach the up-curved liquid surface at O_1 and O_2, respectively. In particular, the reflective ray 2′ and incident ray 4 are the boundary rays and just pass through the critical height of the up-curved liquid surface. There will be no reflection in the range between rays 2′ and 4′ and they form a dark region on the observation, which was shown in Fig. 5. In order that the boundary rays 2 and 4 reflect from the free liquid surface, the glancing angle of the incident ray is chosen to be as small as possible.

According to the above theoretical analysis, the optical measurement can be shown in Fig. 5. From the geometry of Fig. 5, the relation of the critical height of the up-curved liquid surface, the dark region width on the screen, the diameter of the rod, and the glancing angle are simply derived. Thus, the relationship can be written in the form as follows:

$$h = \frac{l}{2} - \frac{d}{2} \tan \varphi, \tag{2}$$

where h is the relation of the critical height of the up-curved liquid surface, l is the dark region width on the screen, d is the rod diameter, and φ is the glancing angle.

The Wilhelmy rod technique is an alternative method in which the contact angle is determined by measuring the critical height/depth of the dynamic curved liquid surface around the vertical rod. In this method, the dynamic contact angle is determined from the critical depth/height of the dynamic liquid surface according to [20,21]

$$\sin \theta = 1 - \frac{(\rho_l - \rho_g) g h^2}{2\gamma}, \tag{3}$$

where θ is the dynamic contact angle of the dynamic curved liquid surface, ρ_l is the density of the liquid, ρ_g is the density of the gas phase above the liquid, g is the acceleration due to gravity, h is the critical depth/height of the dynamic liquid surface, and γ is the surface tension.

For the down-curved liquid surface, the relation of the contact angle of the down-curved liquid surface and the angle between the water surface normal and the tangent at the depth point of the down-curved liquid surface can be written in the form as follows:

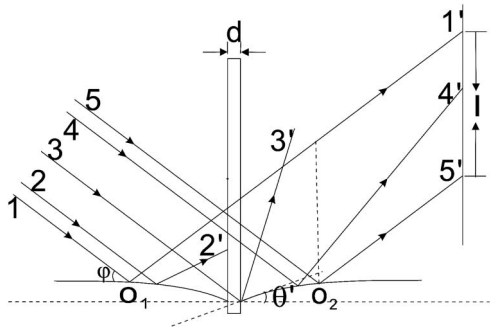

Fig. 4. Schematic diagram of glancing incidence by down-curved surface.

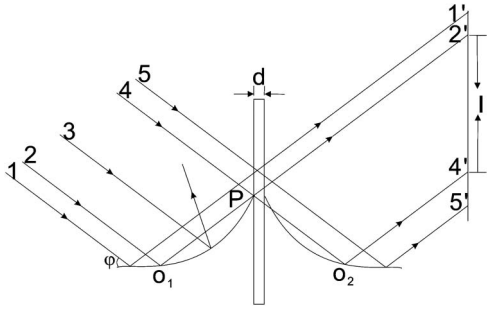

Fig. 5. Schematic diagram of glancing incidence by up-curved surface.

$$\theta_D = \frac{\pi}{2} + \theta', \tag{4}$$

where θ_D is the contact angle of the down-curved liquid surface.

By substituting Eq. (4) for θ' in Eq. (1) and substituting the above result for h into Eq. (3), we can obtain the relation between θ_D and the bright region width of the reflection pattern as

$$\sin\theta_D = 1 - \frac{(\rho_l - \rho_g) g \tan^2\left(\frac{\varphi}{2}\right) l^2}{2\gamma\left[\tan(\varphi + 2\theta_D - \pi) - \tan\left(\frac{\varphi}{2}\right)\right]^2}, \tag{5}$$

where l is the bright region width of reflection pattern.

For the up-curved liquid surface, substituting Eq. (2) for h into Eq. (3), the relation between the contact angle of the up-curved liquid surface and the critical height of the up-curved liquid surface can be obtained in the same manner:

$$\sin\theta_U = 1 - \frac{(\rho_l - \rho_g) g (l - d\ \tan\varphi)^2}{8\gamma}. \tag{6}$$

Here θ_U represents the contact angle of the up-curved liquid surface, and l represents the dark region width of the reflection pattern.

We have discussed the relation between the special patterns and the dynamic curved liquid surface using geometric optics. When the liquid surface becomes curved up, as shown in Fig. 5, the width of the dark region increases with the increasing height of up-curved liquid surfaces. When the liquid surface becomes curved down, as shown in Fig. 4, the width of the bright region increases with the increasing depth of the down-curved liquid surfaces.

We consider calculating the advancing contact angle θ_A of the immersed rod. The advancing contact angle is obtained by substituting θ_A for θ_U into Eq. (6) within 15 s of an immersed rod. We substitute θ_A for θ_U into Eq. (6) at 30 s of an immersed rod. The advancing contact angle, right, which is shown in Fig. 2(b), has been obtained. We substitute θ_A for θ_D into Eq. (5) at 30 s of an immersed rod. The advancing contact angle, left, which is shown in Fig. 2(b), has also been obtained. The advancing contact angles are obtained by substituting θ_A for θ_D into Eq. (5) from 45 s to 120 s of an immersed rod.

Next, we consider calculating the receding contact angle θ_R of a withdrawn rod. The receding contact angles are obtained by substituting θ_R for θ_D into Eq. (5) from 135 s to 150 s of a withdrawn rod. The receding contact angle is obtained by substituting θ_R for θ_U into Eq. (6) from 165 s to 240 s of a withdrawn rod.

The different depths/heights needed for the calculation of the contact angle of the dynamic curved liquid surface on the vertical immersed/withdrawn rod are presented.

4. MEASUREMENT OF THE DYNAMIC CONTACT ANGLE

We have tabulated the measured values of the dynamic contact angle for different l by laser reflection in Tables 1 and 2. In our experiment, the CCD captures the reflection patterns on the screen, and l is determined by the computer. A careful and accurate measurement of l (of the order of 0.01 mm) is crucial for calculating the dynamic contact angle θ. To reduce the systematic error in measuring l, we measure l at least three times. The values of l are obtained by averaging these data. For the immersed rod, using Eq. (2), the critical height h of the up-curved liquid surface is obtained, and from Eq. (6), the value of the advancing contact angle θ_A is calculated at 15 s. We use Eqs. (2) and (6) at 30 s of the immersed rod. The critical height h and advancing contact angle θ_A, right, which are shown in Fig. 2(b), have been obtained, respectively. We use Eq. (5), [1,4] at 30 s of an immersed rod. The critical depth h and advancing contact angle θ_A, left, which are shown in Fig. 2(b), have also been obtained, respectively. From Eq. (5), the value of the advancing contact angle θ_A is calculated, and substituting θ_A for θ_D into Eq. (4), then substituting $\theta_A - \pi/2$ for θ' into Eq. (1), the critical depth h of the down-curved liquid surface is obtained between 45 s and 120 s every 15 s for five intervals. We use the widely accepted values of the parameters $\rho_g = 1.27\ \text{kg/m}^3$, $g = 9.8\ \text{m/s}^2$, $\gamma = 72.8\ \text{mN/m}$, and $\rho_l = 998.23\ \text{kg/m}^3$ for the distilled water in Eqs. (5) and (6) at 20°C. These results are summarized in Table 1. When the liquid surface curved down at the maximum depth, we achieved that the advancing contact angle of dynamic wetting the iron rod by laser reflection is 105.49°. The experimental points (a), shown in Fig. 6, are plotted by using t and the advancing contact angles θ_A in Table 1. And the experimental points (c), shown in Fig. 6, are plotted by using h and the advancing contact angles θ_A in Table 1. Figure 6 shows the fitting curve (b) of the relation between the advancing contact angle θ_A and t, and also shows the fitting curve (d) of the relation between the advancing contact angle θ_A and h through the origin.

Table 1. Value of Advancing Contact Angles as a Rod is Immersed into a Liquid Bath

t (s)	l (mm)	h (mm)	θ_R (deg)
15	2.2748	1.1024	66.68
30	3.6446/1.3453	−0.4215/0.6377	98.92/76.59
45	7.6316	−0.6054	102.84
60	10.2000	−0.6938	104.71
75	10.8115	−0.7126	105.10
90	11.2151	−0.7247	105.36
105	11.4108	−0.7304	105.48
120	11.4230	−0.7308	105.49

Table 2. Value of Receding Contact Angles as a Rod is Withdrawn Out of a Liquid Bath

t (s)	l (mm)	h (mm)	θ_R (deg)
135	8.1942	−0.6262	103.28
150	6.6532	−0.5669	102.02
165	1.4309	0.6805	75.67
180	2.0302	0.9801	69.30
195	2.2626	1.0963	66.81
210	2.4460	1.1880	64.84
225	3.1432	1.5366	57.28
240	3.2410	1.5855	56.21

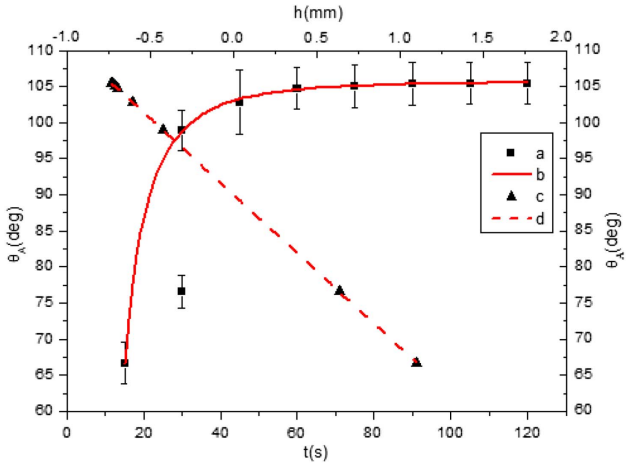

Fig. 6. Measured advancing contact angles with the optical method: h, the height/depth of dynamic curved liquid surface; t, the time; θ_A, the advancing contact angles. (a) represents the value of θ_A at different t (s); (b) is the fitting curve of the relation between θ_A and t; (c) represents the value of θ_A at different h (mm); (d) is the fitting line of the relation between θ_A and h (mm).

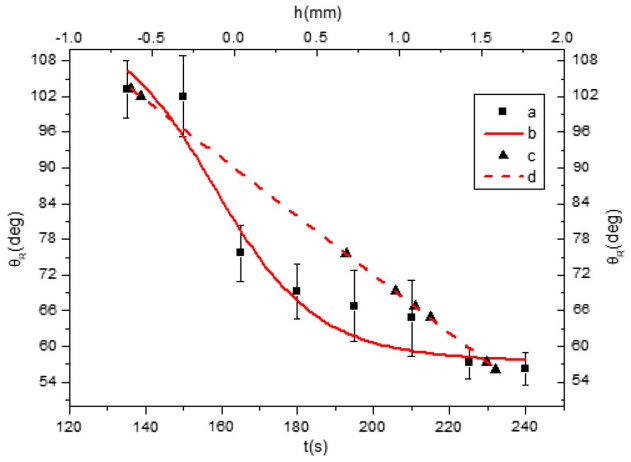

Fig. 7. Measured receding contact angles with the optical method: h, the height/depth of dynamic curved liquid surface; t, the time; θ_R receding contact angles. (a) represents the value of θ_R at different t (s); (b) is the fitting curve of the relation between θ_R and t; (c)represents the value of θ_R at different h (mm); (d) is the fitting line of the relation between θ_R and h (mm).

In Fig. 6, the fitting curve (b) equation is $\theta_A = 105.769 + (-3688.23 - 105.768)/(1 + (t/2.44181)^{2.51478})$ and the goodness-of-fit value is $R^2 = 0.99984$; the fitting line (d) equation is $\theta_A = 90.03015–21.152h$ and the goodness-of-fit value is $R^2 = 1$. The experimental data, shown in Fig. 6, deviates from the fitting curve (b) at 30 s. It is due to one part of the liquid surface from being up-curved to becoming down-curved; another part of the liquid surface is still up-curved but the critical height declined at 30 s.

Next, for the withdrawn rod, from Eq. (5), the value of the receding contact angle θ_R is calculated, and substituting θ_R for θ_D into Eq. (4), then substituting $\theta_R - \pi/2$ for θ' into Eq. (1), the critical depth h of the down-curved liquid surface is obtained at 135 and 150 s. Using Eq. (2), the critical height h of the up-curved liquid surface is obtained, and from Eq. (6), the value of the receding contact angle θ_R is calculated between 165 s and 240 s every 15 s for five intervals. We use the widely accepted values of the parameters $\rho_g = 1.27$ kg/m^3, $g = 9.8$ m/s^2, $\gamma = 72.8$ mN/m, and $\rho_l = 998.23$ kg/m^3 for the distilled water in Eqs. (5) and (6) at 20°C. These results are summarized in Table 2. When the liquid surface curved up at the maximum height, we achieved that the receding contact angle of dynamic wetting the iron rod by laser reflection is 56.21°. The experimental points (a), shown in Fig. 7, are plotted by using t and the receding contact angles θ_R in Table 1. And the experimental points (c), shown in Fig. 7, are plotted by using h and the receding contact angles θ_R in Table 1. Figure 7 shows the fitting curve (b) of the relation between the advancing contact angle θ_R and t, and also shows the fitting line (d) of the relation between the advancing contact angle θ_R and h through the origin.

In Fig. 7, the fitting curve (b) equation is $\theta_R = 57.38253 + (112.5397 - 57.38253)/(1 + (t/159.759)^{12.35915})$ and the goodness-of-fit value is $R^2 = 0.96384$; the fitting line (d) equation is $\theta_R = 90.02398–21.24344h$ and the goodness-of-fit value is $R^2 = 0.99997$. The experimental data, shown in Fig. 7, are evenly distributed around the fitting curve (b). When a rod is vertically withdrawn out of liquid water, the liquid surface will vibrate slightly. The experimental data approximate to the fitting curve (b), while the critical height of the up-curved liquid surface increases. So, the perturbation has a very weak effect on the results of laser reflection.

5. VISUALIZATION OF DYNAMIC CURVED LIQUID SURFACE

The differential equation, which is applicable to our experiment in which the dynamic shape of the surface is described for symmetric figure of plane, may be derived easily. The Young–Laplace equation [21,22],

$$\Delta P = \gamma\left(\frac{1}{R_h} + \frac{1}{R_v}\right), \tag{7}$$

must apply continuously on the profile depicted in Figs. 4 and 5 as a rod is immersed into and then withdrawn out the liquid, where ΔP represents the difference in pressure between the liquid inside and outside the liquid, R_h and R_v are the principal radii of curvature on horizontal and vertical planes, respectively, and γ is the surface tension of the liquid. From analytical geometry, the radii of curvature may be represented by the following equations in terms of Cartesian coordinates:

$$\frac{1}{R_h} = \frac{y''}{(1 + y'^2)^{3/2}}, \qquad \frac{1}{R_v} = \frac{y'}{x(1 + y'^2)^{1/2}}. \tag{8}$$

Here x and y represent horizontal and vertical positions on the profiles, y' and y'' denote the first and second derivations with respect to x.

The pressure difference ΔP may be replaced by $\rho g y$, where ρ is the liquid density and g is the acceleration of gravity. The symbol y represents the height above what would be the surface of the free liquid. Thus, this differential equation for a symmetric figure of revolution may be written as

$$\frac{\rho g y}{\gamma} = \frac{y''}{(1+y'^2)^{3/2}} + \frac{y'}{x(1+y'^2)^{1/2}}. \quad (9)$$

We have listed the height/depth h and the advancing contact angle θ_A in Table 1, and the height/depth h and the receding contact angle θ_R in Table 2. For the immersed rod, the slope of the dynamic curved liquid surface $y' = \tan(\theta_A)$ at $x = x_0$. For the withdrawn rod, the slope of the dynamic curved liquid surface $y' = \tan(\theta_R)$ at $x = x_0$. Thus the angle θ_R/θ_A at $x = x_0$, named the receding/advancing contact angle, which the liquid profile makes with the solid surface at the contact point.

Here, x_0 represents the rod radius ($x_0 = d/2$). So we may obtain three boundary conditions of the immersed rod: $y = h$, $y' = \tan(\theta_A)$ at $x = d/2$; and we also may obtain three boundary conditions of the withdrawn rod: $y = h$, $y' = \tan(\theta_R)$ at $x = d/2$. Generally speaking, the solution of Eq. (9) might be reached under these three boundary conditions.

When a rod is immersed into the liquid bath, a plot of the dynamic curved liquid surface profile versus the horizontal position x is shown in Fig. 8, and when a rod is withdrawn out the liquid bath, a plot of the dynamic curved liquid surface profile versus the horizontal position x is shown in Fig. 9. We can solve second-order differential equations by the Runge–Kutta method of MATLAB software. It must be integrated numerically. Figures 8 and 9 show the numerical calculation result of the water surface profile predicted by Eq. (9), where the bold vertical line at the original describes the rod. The integration uses the surface height/depth h for liquid water in the experiment, which was determined by utilizing Eqs. (1)–(3). The surface tension γ is 72.8 mN/m and the water density ρ_l is 998.23 kg/m^3. The rod in the experiment is made of copper and its radius is $x_0 = 0.40$ mm. It is known from this theoretical profile that the dynamic contact angle in this symmetric revolution case can be determined from the slope of this profile at $x = x_0$.

Finally, the experiment reflected pattern was compared to simulation. We have analyzed the experimental results of the

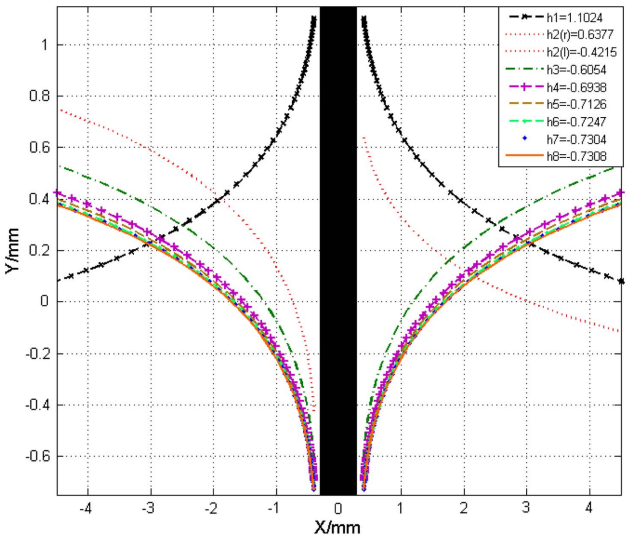

Fig. 8. Numerical calculation result of the dynamic curved surface profile as a rod is immersed into a liquid bath: X, distance from the rod; Y, height/depth of the dynamic curved surface.

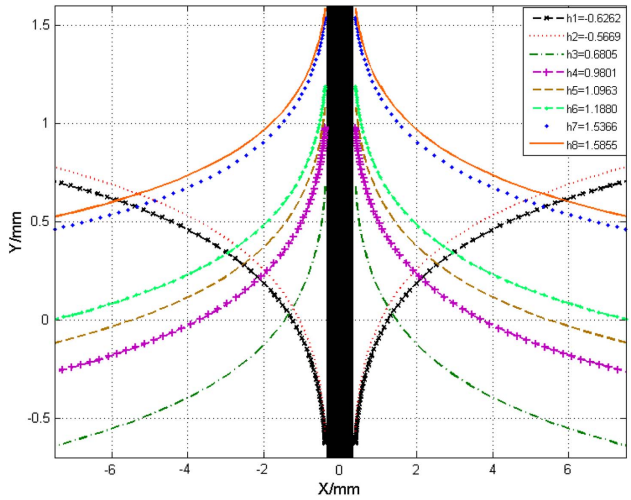

Fig. 9. Numerical calculation result of the dynamic curved surface profile as a rod is withdrawn out of a liquid bath: X, distance from the rod; Y, height/depth of the dynamic curved surface.

immersed rod in Section 3. The reflected pattern, shown in Fig. 2(a), reflects from the up-curved liquid surface in Section 3. The simulation liquid surface profile, shown in Fig. 8 ($h_1 = 1.1024$), is the up-curved liquid surface. The reflected pattern, right, which is shown in Fig. 2(b), reflects from the up-curved liquid surface. The simulation liquid surface profile, right, is shown in Fig. 8 ($h_2(r) = 0.6377$), is the up-curved liquid surface. And the reflected pattern, left, which is shown in Fig. 2(b), reflects from the down-curved liquid surface. The simulation liquid surface profile, right, shown in Fig. 8 ($h_2(l) = -0.4215$), is the down-curved liquid surface. The reflected patterns, which are shown in Figs. 2(c)–2(h), reflect from the down-curved liquid surface, respectively. The simulation liquid surface profiles, shown in Fig. 8 (h_3-h_8), are down-curved liquid surfaces, respectively. The reflected patterns, shown in Fig. 2, corresponding to the simulation dynamic liquid surface profiles in Fig. 8, one by one are determined.

Next, we have analyzed experimental results of the immersed rod in Section 3. The reflected patterns, which are shown in Figs. 3(a) and 3(b), reflect from the down-curved liquid surface, respectively. The simulation liquid surface profiles, shown in Fig. 9 (h_1-h_2), are the down-curved liquid surfaces, respectively. The reflected patterns, shown in Figs. 3(c)–3(h), reflect from the up-curved liquid surface, respectively. The simulation liquid surface profiles, shown in Fig. 9 (h_3-h_8), are the up-curved liquid surfaces, respectively. The reflected patterns, shown in Fig. 3, also corresponding to simulation dynamic liquid surface profiles in Fig. 9, one by one are determined. Through comparative study, it could confirm the simulation results fit the experimental data well.

6. CONCLUSION

In conclusion, we developed an optical measuring method that can determine the dynamic contact angles and the changes of the dynamic curved liquid surface by using the width of the dark/bright region automatically formed by the dynamic

curved liquid surface. The relationship between and the dark (bright) region width on the screen was theoretically derived. By analyzing the relation between the critical height of the up-curved (down-curved) liquid surface and the dynamic contact angle, we calculated the value of the dynamic contact angle. Furthermore, the profile of the dynamic curved liquid can be obtained. Actual measurements have verified the validity and usefulness of this method. Finally, this method is particularly suitable for measurement of single fiber contact angle. It should also be noted that the rod, inserted into the liquid and withdrawn out, should be in the vertical direction strictly, and the laser beam must be collimated. Otherwise, inaccurate experimental results may be produced.

REFERENCES

1. A. E. El Ghzaoui, "Determination of contact angles: consistency between experiment and theory," J. Appl. Phys. **86**, 2920–2922 (1999).
2. W. Jin, J. Koplik, and J. R. Banavar, "Wetting hysteresis at the molecular scale," Phys. Rev. Lett. **78**, 1520–1523 (1997).
3. Y. L. Chen, C. A. Helm, and J. N. Israelachvili, "Molecular mechanisms associated with adhesion and contact angle hysteresis of monolayer surfaces," J. Phys. Chem. **95**, 10736–10747 (1991).
4. X. D. Wang, X. F. Peng, J. Min, and T. Liu, "Hysteresis of contact angle at liquid-solid interface," J. Basic Sci. Eng. **9**, 43–353 (2001).
5. Z. G. Zhao, "Contact angle and its application in surface chemistry," Chem. Res. Appl. **12**, 370–374 (2000).
6. F. Zhu, R. Miao, and Y. Zhang, "A contact angle measurement by laser glancing incidence method," J. Appl. Phys. **104**, 063112 (2008).
7. J. F. Padday, A. R. Pitt, and R. M. Pashley, "Menisci at a free liquid surface: surface tension from the maximum pull on a rod," J. Chem. Soc. Faraday Trans. 1 **71**, 1919–1931 (1975).
8. N. Kaiser, A. Cröll, F. R. Szofran, S. D. Cobb, and K. W. Benz, "Wetting angle and surface tension of germanium melts on different substrate materials," J. Cryst. Growth **231**, 448–457 (2001).
9. F. Zhu and R. C. Miao, "Study on boundary light reflection from curved liquid surface by the wetting rod," Laser J. **28**, 72–73 (2007) (in Chinese).
10. K. Katoh, T. Yu, M. Yamamoto, T. Azuma, and H. Fujita, "A new method for measuring contact angle and liquid surface tension applying detachment of two-dimensional meniscus," J. Colloid Interface Sci. **202**, 54–62 (1998).
11. P. G. Petrov and J. G. Petrov, "Extrapolated dynamic contact angle and viscous deformation of a steady moving meniscus at a vertical flat wall," Langmuir **11**, 3261–3268 (1995).
12. I. Aranberri-Askargorta, T. Lampke, and A. Bismarck, "Wetting behavior of flax fibers as reinforcement for polypropylene," J. Colloid Interface Sci. **263**, 580–589 (2003).
13. J. I. Yamaki and Y. Katayama, "New method of determining contact angle between monofilament and liquid," J. Appl. Polym. Sci. **19**, 2897–2909 (2010).
14. H. Kim and J. P. Rothstein, "Dynamic contact angle measurements of viscoelastic fluids," J. Non-Newtonian Fluid Mech. **225**, 54–61 (2015).
15. R. Miao, Z. Yang, and J. Zhu, "Critical light reflection from curved liquid surface," Opt. Commun. **218**, 199–203 (2003).
16. J. Dong, R. Miao, and J. Qi, "Visualization of the curved liquid surface by means of the optical method," J. Appl. Phys. **100**, 124914 (2006).
17. F. Zhu and R. Miao, "Boundary reflection from curved liquid surfaces and its application," Opt. Commun. **275**, 288–291 (2007).
18. A. Rößler, "Second order Runge–Kutta methods for Itô stochastic differential equations," SIAM J. Numer. Anal. **47**, 1713–1738 (2009).
19. F. Yuan, Z. Wang, X. Yu, Z. Wei, S. Li, and J. Wang, "Visualization of the formation of interfacially polymerized film by an optical contact angle measuring device," J. Phys. Chem. C **116**, 11496–11506 (2012).
20. G. Gu, D. Li, and P. Cheng, "A novel contact angle measurement technique by analysis of capillary rise profile around a cylinder (ACRPAC)," Colloids Surf. A **122**, 135–149 (1997).
21. A. W. Adamson, "Capillarity," in *Physical Chemistry of Surfaces* (Science, 1984), pp. 21–23 (in Chinese).
22. J. J. Bikerman, "Wetting," in *Physical Surface* (Academic, 1970), pp. 239–296.